Available online at www.eccomasproceedia.org
Eccomas Proceedia COMPDYN (2023) 3394-3403

ECCOMAS
Proceedia

COMPDYN 2023
9th ECCOMAS Thematic Conference on
Computational Methods in Structural Dynamics and Earthquake Engineering
M. Papadrakakis, M. Fragiadakis (eds.)
Athens, Greece, 12-14 June 2023

STRUCTURAL DEFORMATION RECONSTRUCTION USING THE HYBRID SHELL-BEAM INVERSE FINITE ELEMENT METHOD: THEORY & NUMERICAL RESULTS

Rinto Roy[1], Marco Esposito[2], Marco Gherlone[2], and Cecilia Surace[1]

[1] Department of Structural, Geotechnical and Building Engineering, Politecnico di Torino,
Corso Duca degli Abruzzi, 24, 10129 Torino, Italy
e-mail: {rinto.roy,cecilia.surace}@polito.it

[2] Department of Mechanical & Aerospace Engineering, Politecnico di Torino,
Corso Duca degli Abruzzi, 24, 10129 Torino, Italy
e-mail: {marco.esposito,marco.gherlone}@polito.it

Abstract. *This work introduces a robust and computationally efficient method for reconstructing the full-field elastic deformations of thin-walled and stiffened panel structures using discrete strain-sensor measurements. The approach presented is based on the inverse Finite Element Method (iFEM), a variationally-based shape sensing technique that attempts to reconstruct the structural displacements by matching a set of experimental and analytically defined strains in a least-squares sense. The novelty of the present work is the introduction of a hybrid discretisation paradigm for the iFEM whereby both beam and shell inverse finite elements are conjointly used to model the structure and capture its deformations. The theoretical framework for this new method and the kinematic coupling between shell and beam inverse elements, proposed based on the first-order shear deformation theory, is presented. Adoption of such a hybrid discretization scheme reduces the number of inverse elements required for structural modelling, thereby reducing computational time and effort. Additionally, beam elements reduce the number of in-situ strain sensors required compared to a solely shell-based inverse model. The hybrid iFEM approach is demonstrated numerically for the shape sensing of a stiffened panel under different load conditions. The preliminary results are accurate and efficient, demonstrating the capabilities of the hybrid iFEM as a potential monitoring approach, especially for aerospace applications where high strength and low mass requirements have led to the widespread adoption of thin-walled and stiffened structural geometry designs.*

Keywords: Inverse Methods, Shape Sensing, Beam-Shell Models, Stiffened Panel

ISSN:2623-3347
Peer-review under responsibility of the organizing committee of COMPDYN 2023.
doi: 10.7712/120123.10647.20632

1 INTRODUCTION

Inverse problems in structural engineering are key to estimating important characteristics of a structure when only indirect measurements are available. Reconstructing structural displacements in real-time from discrete strains, termed shape sensing, is such an inverse problem with the potential for real-time damage diagnosis and prognosis in the domain of Structural Health Monitoring (SHM) [1]. However, inverse problems are ill-posed, requiring efficient methods to ensure accurate, unique, and stable solutions. Although solution approaches to shape sensing based on strain integration, basis functions, and neural networks have been proposed in literature [2], those using a variational principle, such as the inverse Finite Element Method (iFEM) [3], have perhaps found the widest acceptance.

Displacement reconstruction using the iFEM is based on solving a functional defined as the least-squares error between analytical and experimental strains. The two main ingredients of the iFEM are the adoption of the finite element discretisation framework and the use of interpolation functions and the strain-displacement relations to approximate the analytical strains. The former allows complex geometries to be modelled, while the latter ensures that the iFEM is inherently independent of the material properties or loading conditions of the structure. iFEM developments have primarily focused on novel inverse element formulations to model one-dimensional (1D) beam and frame structures (called 1D iFEM) or two-dimensional (2D) plate or shell structures (called 2D iFEM). In the context of the 2D iFEM, the three- and four-node Mindlin shell [4, 5], eight-node curved shell [6], and multi-layered composite [7] elements have been developed and applied for monitoring aerospace, civil, or marine structures involving metallic and composite constructions [8, 9, 10]. When analysing complex structures, a precise 2D iFEM model involving a high-fidelity inverse shell element discretisation can be used to obtain accurate results. However, in this case, the analysis is computationally intensive, requiring strain measurements from a relatively large number of sensors instrumented on the structure. In contrast, the 1D iFEM offers a low-cost (computational and sensor) alternative for monitoring beam or frame structures, with inverse elements for thick [11] and thin beams [12], complex cross-sectional beams [13], and composite structures [14] comprising the major developments. They have also been applied for various aerospace [15] and marine structures [16]. As the 1D iFEM uses a low-fidelity finite beam element discretisation, the validity of the results is highly dependent on the kinematic relations used. As geometric complexity increases, the assumptions can break down, leading to inaccurate results. Hence, neither 1D nor 2D iFEM offers an optimal solution between accuracy, computational cost, and sensor requirement for monitoring structures such as a stiffened panel or a wing box.

This work proposes a solution to this problem by developing a hybrid iFEM scheme where the structure is discretised using both beam and shell elements. Such a coupling ensures greater accuracy than the 1D iFEM, while requiring fewer strain measurements and computational effort than the 2D iFEM. The hybrid iFEM is applied in this work for the numerical shape sensing of a cantilevered stiffened panel instrumented with fibre optic sensors. As per the hybrid scheme, the flat panel is discretised using shell elements, and the stringers use beams. The iFEM accuracy in reconstructing the bending and twisting deformation of the panel is evaluated by comparing results with a high-fidelity finite element (FE) model of the structure. The paper is organised as follows: the theoretical formulation of the hybrid iFEM is given in Section 2. The hybrid iFEM is demonstrated numerically in Section 3 for the shape sensing of a stiffened panel under different loading conditions. Finally, Section 4 concludes with the main conclusions and opportunities for future work.

2 HYBRID INVERSE FINITE ELEMENT METHOD

The 1D and 2D iFEM formulations, proposed by Gherlone et al. [11] and Tessler et al. [3], respectively, are briefly recollected in this section. Subsequently, the theoretical formulation of the hybrid iFEM is presented.

2.1 1D Inverse Finite Element Method

The 1D iFEM for beams or frames is based on the kinematic assumptions of Timoshenko beam theory [11], where the kinematic variables $\mathbf{u}_b \equiv \{u, v, w, \theta_x, \theta_y, \theta_z\}^T$ are used to describe the Cartesian components of the displacement vector as

$$u_x(\mathbf{x}) = u(x) + z\theta_y(x) - y\theta_z(x) \;\;,\;\; u_y(\mathbf{x}) = v(x) - z\theta_x(x) \;\;,\;\; u_z(\mathbf{x}) = w(x) + y\theta_x(x) \quad (1)$$

where the kinematic variables, u, v, and w, are the beam displacements at the shear centre along the x, y and z-axis, respectively (see Fig. 1), and θ_x, θ_y, and θ_z are the torsional and bending rotations about the x, y, and z-axis, respectively.

Using the linear strain-displacement relations, the corresponding strain field is computed

$$\begin{Bmatrix} \varepsilon_x(\mathbf{x}) \\ \gamma_{xz}(\mathbf{x}) \\ \gamma_{xy}(\mathbf{x}) \end{Bmatrix} = \begin{Bmatrix} u_{x,x} \\ u_{x,z} + u_{z,x} \\ u_{x,y} + u_{y,x} \end{Bmatrix} = \begin{Bmatrix} e_1(x) + ze_2(x) + ye_3(x) \\ e_4(x) + ye_6(x) \\ e_5(x) - ze_6(x) \end{Bmatrix} \quad (2)$$

where e_i $(i = 1, ..., 6)$ are the sectional strains defined along the beam axis. Using element shape functions to interpolate the nodal degrees-of-freedom (DOF) and approximate the displacements and strains within an element, the sectional strains can be written as

$$\begin{aligned} \mathbf{e}(\mathbf{u}_b) &= \{e_1, e_2, e_3, e_4, e_5, e_6\}^T \\ &= \{u_{,x}, \theta_{y,x}, -\theta_{z,x}, w_{,x} + \theta_y, v_{,x} - \theta_z, \theta_{x,x}\}^T = \mathbf{B}^s \mathbf{u}_b^e \end{aligned} \quad (3)$$

where $\mathbf{B}^s$ is a matrix of shape function derivatives and $\mathbf{u}_b^e$ is the nodal DOF vector of the element.

Although Eq. 3 provides the analytical form of the sectional strains, they can also be computed experimentally from strain measurements. For a strain sensor instrumented at an axial location x_i and orientation β on the beam surface, the surface strain measurement can be written in terms of the experimental sectional strains, $\mathbf{e}^\epsilon = \{e_1^\epsilon, e_2^\epsilon, e_3^\epsilon, e_4^\epsilon, e_5^\epsilon, e_6^\epsilon\}^T$ as [13]

$$\begin{aligned} \varepsilon^*(x_i, c, \beta) = (e_1^\epsilon(x_i) + e_2^\epsilon(x_i) z_i + e_3^\epsilon(x_i) y_i) (\cos^2\beta - \nu \sin^2\beta) + \\ \left(\frac{1}{k_{\epsilon z}} e_4^\epsilon(x_i) f_1(y_i, z_i) + \frac{1}{k_{\epsilon y}} e_5^\epsilon(x_i) f_2(y_i, z_i) + e_6^\epsilon(x_i) f_3(y_i, z_i) \right) \cos\beta \sin\beta \end{aligned} \quad (4)$$

where f_1, f_2, f_3, $k_{\epsilon y}$ and $k_{\epsilon z}$ are functions and coefficients used to model the shear strains variation due transverse or torsional loads and are only a function of the beam profile. Given a discrete set of strain measurements, Eq. 4 can be solved to compute $\mathbf{e}^\epsilon$.

The 1D iFEM is based on the finite element framework where the structural domain is discretised using 1D finite elements. For each element e, a weighted-least-squares error functional can be formulated as

$$\Phi_b^e(\mathbf{u}_b^e) \equiv \mathbf{w}_s \mathbf{\Phi}_s(\mathbf{u}_b^e) \equiv \mathbf{w}_s \sum_{i=1}^{N} \frac{l_e}{N} \left[\mathbf{e}(x_i) - (\mathbf{e}^\epsilon)_i \right]^2 \quad (5)$$

where $\mathbf{w}_s = \{w_k\}$ $(k = 1, ..., 6)$ is a vector of weighing coefficients used to control the enforcement of the least-squares compatibility of each sectional strain component and ensures the dimensional consistency of Eq. 5, l_e is the element length, and N is the total number of axial sections with strain measurements.

Eq. 5 is minimized with respect to the nodal DOF of the element to obtain the following element set of linear algebraic equations

$$\frac{\partial \Phi_b^e(\mathbf{u}_b^e)}{\partial \mathbf{u}_b^e} = \mathbf{k}_b^e \mathbf{u}_b^e - \mathbf{f}_b^e = 0 \rightarrow \mathbf{k}_b^e \mathbf{u}_b^e = \mathbf{f}_b^e \tag{6}$$

where matrix $\mathbf{k}_b^e$ is only a function of the sensor positions while vector $\mathbf{f}_b^e$ is a function of the sensor positions and measured strains. These element matrices can also be written as the weighted sum of contributions from each sectional strain as

$$\mathbf{k}_b^e(\mathbf{u}_b^e) = \sum_{k=1}^{6} w_k \left(\frac{l_e}{N} \sum_{i=1}^{N} \left(\mathbf{B}_k^s(x_i)\right)^T \mathbf{B}_k^s(x_i) \right), \; \mathbf{f}_b^e(\mathbf{u}_b^e) = \sum_{k=1}^{6} w_k \left(\frac{l_e}{N} \sum_{i=1}^{N} \left(\mathbf{B}_k^s(x_i)\right)^T (e_k^\epsilon)_i \right) \tag{7}$$

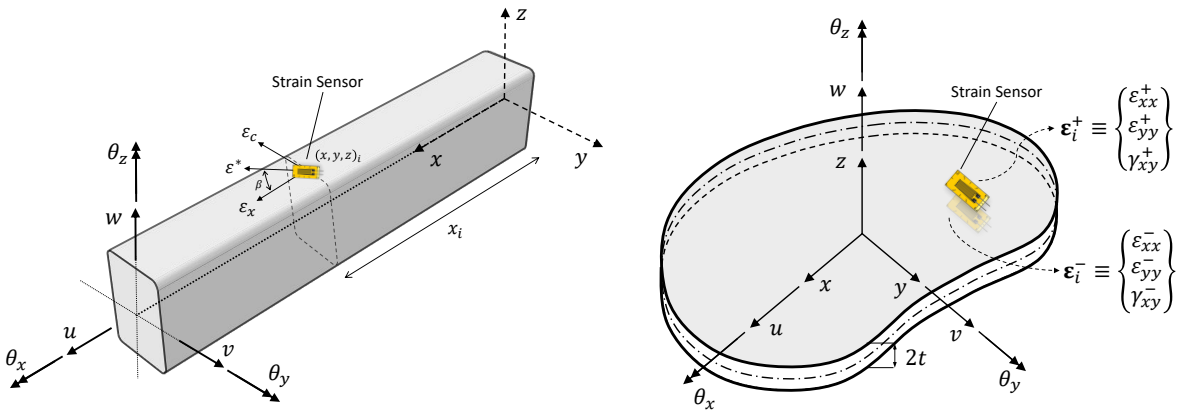

(**a**) (**b**)

Figure 1: Definition of the variables used to define the (a) beam and (b) plate kinematics

2.2 2D Inverse Finite Element Method

The 2D iFEM for plates or shells is formulated based on the kinematic assumptions of Mindlin theory [4], where the kinematic variables $\mathbf{u}_p \equiv \{u, v, w, \theta_x, \theta_y\}^T$ are used to describe the Cartesian components of the displacement vector as

$$u_x = u(\mathbf{x}) + z\theta_y(\mathbf{x}) \quad , \quad u_y = v(\mathbf{x}) - z\theta_x(\mathbf{x}) \quad , \quad u_z = w(\mathbf{x}) \tag{8}$$

where the variables u and v, are the mid-plane displacements in the x and $y-$directions; w is section-averaged transverse deflection; and θ_x and θ_y are the section rotations about the x and y-axes, respectively (see Fig. 1).

The in-plane and transverse shear strains of the plate are computed from Eq. 8 using the linear strain-displacement relations

$$\begin{Bmatrix} \varepsilon_{xx} \\ \varepsilon_{yy} \\ \gamma_{xy} \end{Bmatrix} = \begin{Bmatrix} u_{x,x} \\ u_{y,y} \\ u_{x,y} + u_{y,x} \end{Bmatrix} = \begin{Bmatrix} u_{,x} \\ v_{,y} \\ u_{,y} + v_{,x} \end{Bmatrix} + z \begin{Bmatrix} \theta_{y,x} \\ -\theta_{x,y} \\ -\theta_{x,x} + \theta_{y,y} \end{Bmatrix} = \mathbf{m}(\mathbf{u}_p) + z\mathbf{k}(\mathbf{u}_p)$$
$$\begin{Bmatrix} \gamma_{xz} \\ \gamma_{yz} \end{Bmatrix} = \begin{Bmatrix} u_{z,x} + u_{x,z} \\ u_{z,y} + u_{y,z} \end{Bmatrix} = \begin{Bmatrix} w_{,x} + \theta_y \\ w_{,y} - \theta_x \end{Bmatrix} = \mathbf{g}(\mathbf{u}_p) \tag{9}$$

where **m**, **k**, and **g** are the strain measures defined in the mid-plane surface and representing the membrane, curvature, and transverse shear strain of the mid-plane.

Using element shape functions to interpolate the nodal DOF and approximate the displacements and strains within an element, Eq. 9 can be written as

$$\begin{Bmatrix} \varepsilon_{xx} \\ \varepsilon_{yy} \\ \gamma_{xy} \end{Bmatrix} = \mathbf{m}(\mathbf{u}_p^e) + z\mathbf{k}(\mathbf{u}_p^e) = \mathbf{B}^m\mathbf{u}_p^e + z\mathbf{B}^k\mathbf{u}_p^e \quad , \quad \begin{Bmatrix} \gamma_{xz} \\ \gamma_{yz} \end{Bmatrix} = \mathbf{g}(\mathbf{u}_p^e) = \mathbf{B}^g\mathbf{u}_p^e \tag{10}$$

where $\mathbf{B}^m$, $\mathbf{B}^k$, and $\mathbf{B}^g$ are matrices of shape function derivatives and $\mathbf{u}_p^e$ is the nodal DOF vector. An additional drilling DOF, θ_z, can be introduced in $\mathbf{u}_p^e$ by means of interdependent shape functions (discussed by Kefal et al. [5] for the iQS4 element). Hence, even though θ_z is not one of the kinematic variables of Mindlin theory, it appears among the nodal DOF.

The strain measures of Eq. 10 can also be computed from experimental strain measurements. Using plate top, $\boldsymbol{\varepsilon}_i^+ = \{\varepsilon_{xx}^+, \varepsilon_{yy}^+, \gamma_{xy}^+\}_i^T$, and bottom, $\boldsymbol{\varepsilon}_i^- = \{\varepsilon_{xx}^-, \varepsilon_{yy}^-, \gamma_{xy}^-\}_i^T$, surface strains measured by sensors placed at discrete in-plane locations, $\mathbf{x}_i = (x, y)_i$, the membrane and curvature strain measures can be computed using the relations

$$\mathbf{m}_i^\epsilon = \frac{1}{2}\left(\begin{Bmatrix} \epsilon_{xx}^+ \\ \epsilon_{yy}^+ \\ \gamma_{xy}^+ \end{Bmatrix} + \begin{Bmatrix} \epsilon_{xx}^- \\ \epsilon_{yy}^- \\ \gamma_{xy}^- \end{Bmatrix} \right)_i \quad , \quad \mathbf{k}_i^\epsilon = \frac{1}{2t}\left(\begin{Bmatrix} \epsilon_{xx}^+ \\ \epsilon_{yy}^+ \\ \gamma_{xy}^+ \end{Bmatrix} - \begin{Bmatrix} \epsilon_{xx}^- \\ \epsilon_{yy}^- \\ \gamma_{xy}^- \end{Bmatrix} \right)_i \tag{11}$$

The 2D iFEM uses the finite element framework to discretise the structure using 2D inverse finite elements. For each element, e, a weighted least-squares error functional is formulated as

$$\Phi_p^e(\mathbf{u}_p^e) \equiv \mathbf{w}_m\boldsymbol{\Phi}_m(\mathbf{u}_p^e) + \mathbf{w}_k\boldsymbol{\Phi}_k(\mathbf{u}_p^e) + \mathbf{w}_g\boldsymbol{\Phi}_g(\mathbf{u}_p^e) \tag{12}$$

where $\mathbf{w}_m$, $\mathbf{w}_b$, and $\mathbf{w}_s$, are row vectors of weighting coefficients, while the corresponding error functionals are given as

$$\begin{aligned} \boldsymbol{\Phi}_m &\equiv \frac{1}{A_p^e}\int_{A_p^e}[\mathbf{m}(\mathbf{u}_p^e) - \mathbf{m}^\epsilon]^2 dA \ , \ \boldsymbol{\Phi}_k \equiv \frac{(2t)^2}{A_p^e}\int_{A_p^e}[\mathbf{k}(\mathbf{u}_p^e) - \mathbf{k}^\epsilon]^2 dA \\ \boldsymbol{\Phi}_g &\equiv \frac{1}{A_p^e}\int_{A_p^e}[\mathbf{g}(\mathbf{u}_p^e)]^2 dA \end{aligned} \tag{13}$$

The weighting coefficients are used to specify the correlation between the analytical and experimental strain measurements. They are set to unity ($\mathbf{w}_m = \mathbf{w}_b = \{1, 1, 1\}$) when experimental strains are available for an element and to a small value (10^{-3}–10^{-5}) otherwise to reduce the element contribution from the global functional. As $\mathbf{g}^\epsilon$ cannot be computed directly from experimental measurements, the square norm follows the form of Eq.13 with $\mathbf{w}_g = \{10^{-5}, 10^{-5}\}$.

Minimising Eq. 12 with respect to the nodal DOF gives to rise to the following element set of equations

$$\frac{\partial \Phi_p^e(\mathbf{u}_p^e)}{\partial \mathbf{u}_p^e} = \mathbf{k}_p^e \mathbf{u}_p^e - \mathbf{f}_p^e = 0 \rightarrow \mathbf{k}_p^e \mathbf{u}_p^e = \mathbf{f}_p^e \tag{14}$$

where matrix $\mathbf{k}_p^e$ and vector $\mathbf{f}_p^e$ are given in terms of the shape function derivatives as

$$\begin{aligned} \mathbf{k}_p^e(\mathbf{u}_p^e) &= \frac{1}{A_p^e} \int_{A_p^e} \left[\mathbf{w}_m (\mathbf{B}^m)^T \mathbf{B}^m + \mathbf{w}_k (2t)^2 (\mathbf{B}^k)^T \mathbf{B}^k + \mathbf{w}_g (\mathbf{B}^g)^T \mathbf{B}^g \right] dA, \\ \mathbf{f}_p^e(\mathbf{u}_p^e) &= \frac{1}{A_p^e} \int_{A_p^e} \left[\mathbf{w}_m (\mathbf{B}^m)^T \mathbf{m}^\epsilon + \mathbf{w}_k (2t)^2 (\mathbf{B}^k)^T \mathbf{k}^\epsilon + \mathbf{w}_g (\mathbf{B}^g)^T \mathbf{g}^\epsilon \right] dA. \end{aligned} \tag{15}$$

2.3 Hybrid Formulation

The hybrid iFEM formulation discretises the structure using both beam and shell inverse finite elements. Combining beam, Φ_b, and shell, Φ_p, element contributions, the global error functional of the structure is written as

$$\Phi(\mathbf{u}) \equiv \Phi_b(\mathbf{u}) + \Phi_p(\mathbf{u}) \tag{16}$$

where $\mathbf{u} \equiv \{u, v, w, \theta_x, \theta_y, \theta_z\}^T$ is the vector of kinematic variables.

Minimising Eq. 16 with respect to $\mathbf{u}$ produces the global equations of the structure,

$$\mathbf{KU} = \mathbf{F} \tag{17}$$

where matrix $\mathbf{K}$ and vector $\mathbf{F}$ can be written as the superposition of n_b beam and n_p shell element contributions with the appropriate local-to-global transformations, $\mathbf{T}^e$, as

$$\begin{aligned} \mathbf{K}(\mathbf{u}) &= \mathbf{K}_b(\mathbf{u}) + \mathbf{K}_p(\mathbf{u}) = \sum_{e=1}^{n_b} (\mathbf{T}^e)^T \mathbf{k}_b^e \mathbf{T}^e + \sum_{e=1}^{n_p} (\mathbf{T}^e)^T \mathbf{k}_p^e \mathbf{T}^e \\ \mathbf{U}(\mathbf{u}) &= \mathbf{U}_b(\mathbf{u}) + \mathbf{U}_p(\mathbf{u}) = \sum_{e=1}^{n_b} (\mathbf{T}^e)^T \mathbf{u}_b^e + \sum_{e=1}^{n_p} (\mathbf{T}^e)^T \mathbf{u}_p^e \\ \mathbf{F}(\mathbf{u}) &= \mathbf{F}_p(\mathbf{u}) + \mathbf{F}_b(\mathbf{u}) = \sum_{e=1}^{n_p} (\mathbf{T}^e)^T \mathbf{f}_p^e \mathbf{T}^e + \sum_{e=1}^{n_b} (\mathbf{T}^e)^T \mathbf{f}_b^e \mathbf{T}^e \end{aligned} \tag{18}$$

As in the direct FEM, nodal boundary conditions are used to constrain the structure against rigid-body motion and ensure a non-singular system matrix. Finally, Eq. 17 is solved to obtain the iFEM reconstructed nodal displacements, $\mathbf{U}$, of the structure.

3 NUMERICAL STUDY

The hybrid iFEM formulation is applied for the numerical shape sensing of a cantilevered stiffened panel in this section. The panel is 300 mm long, 180 mm wide, and 2 mm thick and is composed of six longitudinal stringers of rectangular cross-section 2×10 mm^2 (shown in Fig. 2). It is made of an aluminium alloy of Young's Modulus $E = 73$ GPa and Poisson's ratio $\nu = 0.3$. The panel is tested as a cantilever by clamping along one of its short ends. In contrast, the other end is subjected to two different load conditions: a uniformly distributed transverse load that causes the panel to bend and a concentrated transverse load at the corner, causing panel

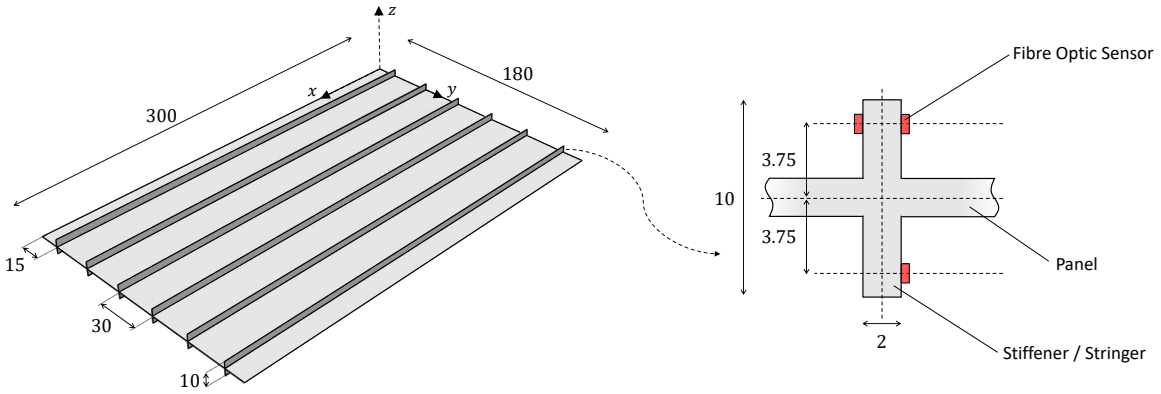

Figure 2: Images of the stiffened panel showing the panel and stringer dimensions, and the location of the fibre optic sensors on each stringer (all dimensions are in mm)

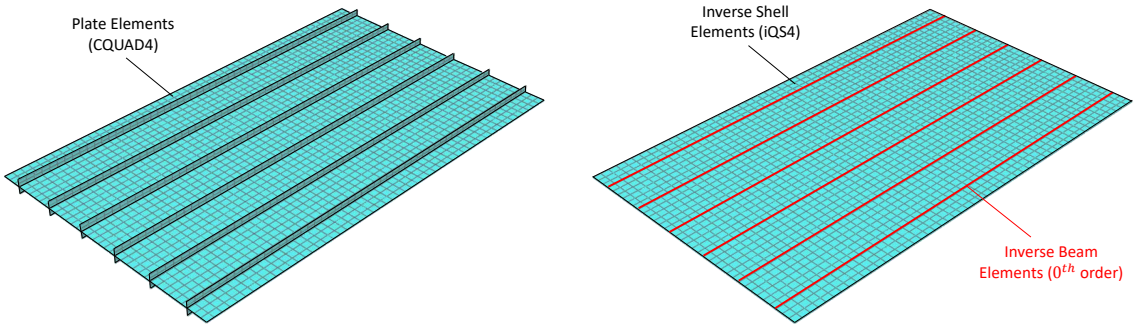

(**a**) (**b**)

Figure 3: The element discretisation for the (a) direct FEM model composed of 3180 CQUAD4 elements, and (b) iFEM model composed of 1908 iQS4 and 318 0^{th}-order beam elements

twisting. The panel is instrumented with a 5.4 m long fibre optic strain sensor to measure the strains during deformation. The fibre is instrumented on the stringers, with each stringer having three sensing lines along which the longitudinal (x-direction) strains are measured.

Given the absence of an experimental model, a high-fidelity finite element (FE) model developed in NASTRAN is used for the present study. The FE strains are inputs for the iFEM analysis, while the FE displacements are the reference for iFEM comparisons. In the direct model, the stiffened panel (including the stringers) is modelled using 3180 CQUAD4 elements, a four-node isoparametric plate element in NASTRAN. The stringers are discretised with 4 subdivisions along their vertical dimension and 53 along their length. The hybrid scheme is adopted for the inverse iFEM model. The flat panel is modelled using 1908 iQS4 elements [5], a four-node inverse shell element with bi-quadratic displacement interpolations and bi-linear rotations, whereas, the stingers are modelled with 318 0^{th}-order inverse beam elements (proposed by Gherlone et al. [11]) with a linear interpolation of axial displacement and torsional rotation, parabolic bending rotations, and cubic transverse deflections. As the fibre optic sensors are instrumented along the stringers, only the beam elements are sensorised in the inverse model.

Hence, the error norms for the shell elements are penalised with a low value of weights (10^{-5}). Additionally, as only longitudinal strains are measured, the transverse shears (e_4 and e_5) and torsional (e_6) sectional strain of the beam cannot be computed directly, and their corresponding weights are set to a small value (10^{-4}).

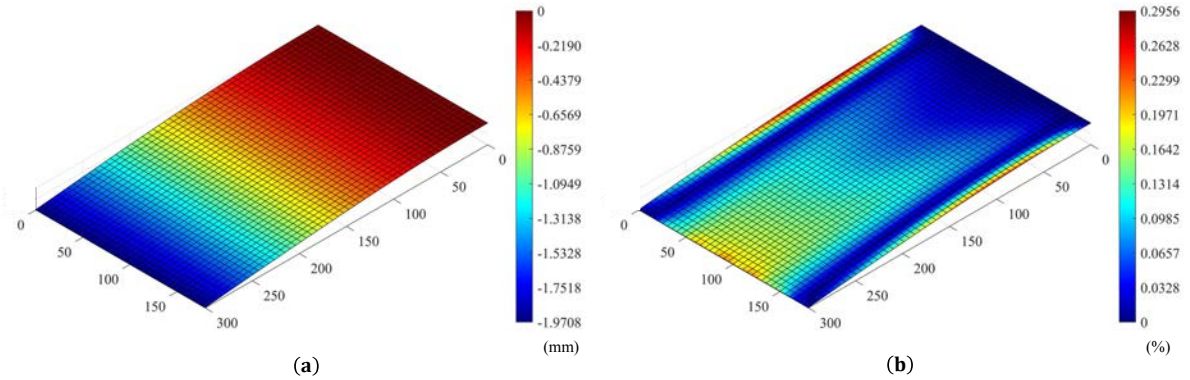

Figure 4: Contour plots of iFEM results for load case 1: (a) w_{iFEM} and (b) w^{err}

The results of the iFEM analysis for load case 1 are given in Fig. 4, where the contour plots of transverse deflection, w_{iFEM}, and its corresponding error, $w^{err} = 100 \times (w_{\text{FE}} - w_{\text{iFEM}})/\{w_{\text{FE}}\}_{max}$, are shown. The iFEM results are seen to be very accurate ($w^{err} < 0.3\%$), with the strains measured on the stringers accurately describing the bending displacements on the panel. The highest errors are at the panel extremities, where local deflection changes might not be captured due to the absence of sensorised elements in its vicinity. Load case 2 presents a more interesting case with the concentrated load causing the panel to twist. Although the beam elements used no information regarding the torsional strain, the differential bending of the stringers accurately captured the global twisting behaviour of the panel ($w^{err} < 0.9\%$ as shown in Fig. 5). In contrast to a complete shell model of the same structures, these results obtained at a low computational cost and relatively lower number of strain measurements indicate the benefits of the hybrid iFEM approach.

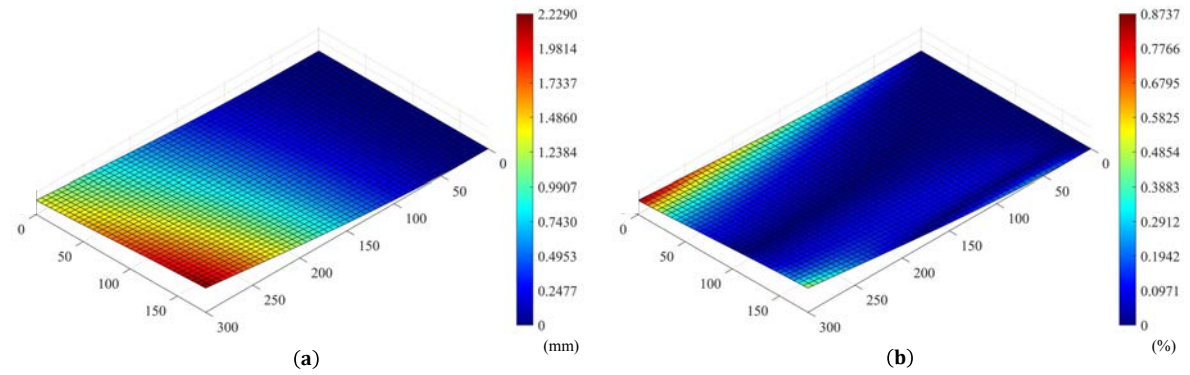

Figure 5: Contour plots of iFEM results for load case 2: (a) w_{iFEM} and (b) w^{err}

4 CONCLUSIONS

This work introduced a hybrid beam-shell inverse Finite Element Method for the accurate, robust, and computationally efficient displacement reconstruction monitoring of thin-walled and stiffened panel structures using discrete strains. The crux of the proposed approach is a novel discretisation paradigm whereby the monitored structure is discretised using both beam and shell inverse finite elements. Such a discretisation scheme reduces the number of inverse elements required for structural modelling, thereby reducing computational time and the number of strain measurements needed. This novel approach was demonstrated for the numerical shape sensing of a cantilevered stiffened panel undergoing bending and twisting deformations. Accurate results were obtained in an efficient manner, highlighting the capabilities of the hybrid iFEM as a structural monitoring tool. Future work aims to combine higher-order inverse elements within this hybrid paradigm and experimentally demonstrate its capabilities for complex structures such as a composite wing box.

REFERENCES

[1] C. R. Farrar and K. Worden. An Introduction to Structural Health Monitoring. *Philosophical Transactions of the Royal Society A: Mathematical, Physical and Engineering Sciences*, 365(1851):303–315, 2007. ISSN 1364503X. doi: 10.1098/rsta.2006.1928.

[2] M. Gherlone, P. Cerracchio, and M. Mattone. Shape sensing methods: Review and experimental comparison on a wing-shaped plate. *Progress in Aerospace Sciences*, 99: 14–26, April, 2018. ISSN 03760421. doi: 10.1016/j.paerosci.2018.04.001. URL https://doi.org/10.1016/j.paerosci.2018.04.001.

[3] A. Tessler and J. L. Spangler. A least-squares variational method for full-field reconstruction of elastic deformations in shear-deformable plates and shells. *Computer Methods in Applied Mechanics and Engineering*, 194(2-5 SPEC. ISS.):327–339, 2005. ISSN 00457825. doi: 10.1016/j.cma.2004.03.015.

[4] A. Tessler and J. Spangler. Inverse FEM for Full-Field Reconstruction of Elastic Deformations in Shear Deformable Plates and Shells. *Proceedings of Second European Workshop on Structural Health Monitoring*, pages 83–90, 2004.

[5] A. Kefal, E. Oterkus, A. Tessler, and J. L. Spangler. A quadrilateral inverse-shell element with drilling degrees of freedom for shape sensing and structural health monitoring. *Engineering Science and Technology, an International Journal*, 19(3):1299–1313, 2016. ISSN 22150986. doi: 10.1016/j.jestch.2016.03.006. URL http://dx.doi.org/10.1016/j.jestch.2016.03.006.

[6] A. Kefal. An efficient curved inverse-shell element for shape sensing and structural health monitoring of cylindrical marine structures. *Ocean Engineering*, 188:106262, 2019. ISSN 00298018. doi: 10.1016/j.oceaneng.2019.106262. URL https://doi.org/10.1016/j.oceaneng.2019.106262.

[7] A. Kefal, A. Tessler, and E. Oterkus. An enhanced inverse finite element method for displacement and stress monitoring of multilayered composite and sandwich structures. *Composite Structures*, 179:514–540, 2017. ISSN 02638223. doi: 10.1016/j.compstruct.2017.07.078. URL http://dx.doi.org/10.1016/j.compstruct.2017.07.078.

[8] E. J. Miller, R. Manalo, and A. Tessler. Full-Field Reconstruction of Structural Deformations and Loads from Measured Strain Data on a Wing Test Article using the Inverse Finite Element Method. *NASA/TM—2016–219407*, 2016.

[9] P. Cerracchio, M. Gherlone, and A. Tessler. Real-time displacement monitoring of a composite stiffened panel subjected to mechanical and thermal loads. *Meccanica*, 50(10): 2487–2496, 2015. ISSN 15729648. doi: 10.1007/s11012-015-0146-8.

[10] M. Esposito and M. Gherlone. Composite wing box deformed-shape reconstruction based on measured strains: Optimization and comparison of existing approaches. *Aerospace Science and Technology*, 99:105758, 2020. ISSN 12709638. doi: 10.1016/j.ast.2020.105758. URL https://doi.org/10.1016/j.ast.2020.105758.

[11] M. Gherlone, P. Cerracchio, M. Mattone, M. Di Sciuva, and A. Tessler. Shape sensing of 3D frame structures using an inverse Finite Element Method. *International Journal of Solids and Structures*, 49(22):3100–3112, 2012. ISSN 00207683. doi: 10.1016/j.ijsolstr.2012.06.009. URL http://dx.doi.org/10.1016/j.ijsolstr.2012.06.009.

[12] P. Savino, M. Gherlone, and F. Tondolo. Shape sensing with inverse finite element method for slender structures. *Structural Engineering and Mechanics*, 72(2):77–87, 2019. doi: https://dx.doi.org/10.12989/sem.2019.72.2.217.

[13] R. Roy, M. Gherlone, and C. Surace. A shape sensing methodology for beams with generic cross-sections: Application to airfoil beams. *Aer. Sci. and Tech.*, 110:106484, 2021. ISSN 1270-9638. URL https://www.sciencedirect.com/science/article/pii/S1270963820311664.

[14] F. Zhao, H. Bao, J. Liu, and K. Li. Shape sensing of multilayered composite and sandwich beams based on Refined Zigzag Theory and inverse finite element method. *Composite Structures*, 261:113321, 2021. ISSN 02638223. doi: 10.1016/j.compstruct.2020.113321. URL https://doi.org/10.1016/j.compstruct.2020.113321.

[15] Y. Zhao, J. Du, Q. Xu, and H. Bao. Real-time monitoring of the position and orientation of a radio telescope sub-reflector with fiber bragg grating sensors. *Sensors (Switzerland)*, 19(3), 2019. ISSN 14248220. doi: 10.3390/s19030619.

[16] Haiming Zhu, Zunfeng Du, and Yougang Tang. Numerical study on the displacement reconstruction of subsea pipelines using the improved inverse finite element method. *Ocean Engineering*, 248:110763, 2022. ISSN 0029-8018. doi: https://doi.org/10.1016/j.oceaneng.2022.110763.